Research Paper

Intracellular ion and protein nanoparticle-induced osmotic pressure modify astrocyte swelling and brain edema in response to glutamate stimuli

JiaRui Zhang[a,b,1], YuXuan Wang[a,b,1], ZiHui Zheng[a,b], XiaoHe Sun[a,b], TingTing Chen[a,b], Chen Li[a,b], XiaoLong Zhang[a,b], Jun Guo[a,b,c,*]

[a] State Key Laboratory Cultivation Base For TCM Quality and Efficacy, School of Medicine and Life Science, Nanjing University of Chinese Medicine, Nanjing 210023, PR China
[b] Key Laboratory of Drug Target and Drug for Degenerative Disease, Nanjing University of Chinese Medicine, Nanjing, PR China
[c] Jiangsu Key Laboratory of Pediatric Respiratory Disease, Institute of Pediatrics, Nanjing University of Chinese Medicine, Nanjing, PR China

ARTICLE INFO

ABSTRACT

Intracellular tension activity plays a crucial role in cytotoxic brain edema and astrocyte swelling. Here, a few genetically encoded FRET-based tension probes were designed to detect cytoskeletal structural tension optically, including their magnitude and vectors. The astrocyte swelling resulted in GFAP tension increment, which is associated with the antagonistic effect of inward microfilaments (MFs) and microtubules (MTs) forces. In glutamate-induced astrocyte swelling, GFAP tension rise resulted from outward ion and protein nanoparticle-induced osmotic pressure (PN-OP) increases, where PN-OP could be elicited by MF and MT depolymerization, protein nanoparticle production, and activation of cofilin and stathmin-1. Attenuation of both ion osmotic pressure and PN-OP by drug combinations, together with free-radical scavenger, relieved cerebral edema in vivo. The study suggests that intracellular osmotic pressure (especially PN-OP) has a pivotal role in glutamate-induced astrocyte swelling and brain edema. Recovery of cytoplasmic potential is a promising target to develop new drugs and cure brain edema.

1. Introduction

Brain edema is defined as an increase in brain water content, which results either from an opening of the blood-brain barrier (vasogenic brain edema) or cell swelling (cytotoxic brain edema) [1]. The cytotoxic brain edema was believed to be mainly caused by swelling of astrocytes, but also includes neurons swell [2–4]. Astrocytes undergo rapid swelling after various acute pathological states, such as cerebral ischemia and traumatic brain injury [5]. The main reason for ischemia-induced astrocytic cell swelling is a disruption of ionic and neurotransmitter homeostasis, particularly the accumulation of glutamate and K^+ in the extracellular space [6–9]. Moreover, free radicals exert their deleterious actions during cytotoxic edema [10]. The extracellular water can flow into the astrocytes predominantly through transmembrane aquaporin (AQP) channels [11], which is driven by the ion (e.g., Na^+, Ca^{2+})

influx and osmotic gradient [12]. Therefore, intracellular tension activity has a crucial role in astrocyte swelling.

Intracellular tension relies on cytoskeletal structure and involves regulation of cell volume and mechanical load bearing [13,14,67]. Osmotic pressure (OP) is generated by differences in chemical potential of ions and colloidal protein particles between the cytoplasm and extracellular fluid [15]. During astrocyte swelling, high OP acts on the membrane and strains the lipid bilayer, leading to an outward pull of intermediate filaments (IFs) in the cytoskeleton through transmembrane binding proteins [16,17]. Other than IFs, microfilaments (MFs) and microfilaments (MTs) are highly polarized cytoskeletal structures. The positively charged ends of MFs are adjoined to the membrane, and negatively charged ends dissociate in the cytoplasm [18,19]. MF tension is generated by the negatively charged-directed motion of myosin, whereas MT tension is dependent upon the movement of dynein and

kinesin [20–22]. Notably, the intracellular structural tension is a vector [23]. Apart from their magnitude, the direction of these tensions may have a greater impact on astrocyte swelling, whereas the individual direction of tensions within the cytoskeletal structure is not known. Moreover, tension due to MFs and MTs could be eliminated if MFs and MTs are depolymerized into actin and tubulin monomers or macromolecular polymers of size 1–100 nm [24,25]. Generation of these proteins may increase colloid OP [26,27]. The influx of ions and water, as well as adjustment of intracellular structural tensions, is involved in astroglial swelling. However, a method to measure the tensions dependent upon the cytoskeleton at the subcellular level has not been well established. Hence, elucidating how intracellular structural tensions participate in mediating astrocyte swelling has been challenging. Recent studies have focused on the molecular mechanisms underlying astrocytic swelling and their signaling pathways, such as aquaporin. Nevertheless, mechanisms of intracellular structural tensions underlying astrocytic swelling remain unclear [28–30].

Glial fibrillary acidic protein (GFAP) is an intermediate filament protein integral to cytoskeletal dynamics regulating the morphology and function of astrocytes [31,32]. We developed a genetically encoded Förster resonance energy transfer (FRET)-based tension probe named "GFAP-cpst-GFAP (GcpG)", where cpst is circularly permuted stretch sensitive FRET. Using the GcpG probe, we measured intracellular tension during astrocyte swelling following the formation of ischemic lesions simulated by glutamate stimuli [33]. Our study affords mechanistic insights into the role of intracellular tension in astrocytic swelling and provides innovative ideas for the clinical treatment of brain edema.

2. Materials and methods

2.1. Cell cultures and reagents

A commercial human glioblastoma U87 cell line was obtained from the American Type Culture Collection (U87-MG, ATCC HTB-14; Manassas, VA, USA). Primary astrocyte cultures were isolated from the cerebral cortex of 24 h-old sucking Sprague–Dawley rats. Before experimentation, cells were removed from culture flasks with trypsin-EDTA (0.25%) (Gibco, Billings, MT, USA) and plated on glass coverslips (diameter = 22 mm) coated with poly-L-lysine. Cells were cultured in Dulbecco's modified Eagle's medium (Gibco, Billings, MT, USA) supplemented with 10% fetal bovine serum (Gibco, Billings, MT, USA), penicillin and streptomycin (Gibco, Billings, MT, USA). Cells were maintained in 5% CO_2 in a humidified atmosphere at 37 °C.

Cytochalasin D and nocodazole were purchased from Sigma-Aldrich (Saint Louis, MO, USA). Glutamate, nimodipine, jasplakinolide, taxol, sennoside A, cantharidin, tamoxifen, and bumetanide were obtained from Sigma-Aldrich (Saint Louis, MO, USA). 2,3-Butanedione monoxime, acetazolamide, caffeine, NaN3, Y-27632, verapamil, and cinepazide maleate were purchased from Invivogen (San Diego, CA, USA). Edaravone and oxiracetam were obtained from Ark Pharmaceuticals (New Delhi, India). Fasudil (HA-1077) was purchased from Shanghai Macklin Biochemicals (Shanghai, China). Ciliobrevin D and ispinesib (SB-715992) were from MedChem Express (Princeton, NJ, USA).

Mouse anti-β-actin or α-tubulin antibodies were purchased from Cell Signaling Technology (Danvers, MA, USA). Rabbit anti-GFAP antibody, Rabbit anti-cofilin antibody, rabbit anti-stathmin-1 antibody, rabbit anti-phospho-cofilin (Ser3) antibody and rabbit anti-phospho-stathmin-1 (Ser16) antibody were from Abcam (Cambridge, UK).

2.2. Probe construction and transfection

Sensors were created using restriction endonuclease cloning methods, in accordance with previous reports [13]. We constructed fluorescent sensors with circularly permutated cpVenus and cpCerulean (cpVenus–7aa–cpCerulean[cpstFRET]). pET-cpstFRET was created by connecting cpVenus to the C-terminal of cpCerulean in pET-52b(+)

vector; primers used were: 5′-GGCGGCAGATCTATGGGCAGCGTGCAG CTCGCC-3′ with BglII and 5′-CCAGAGCGAGCTCGTCCTCGATGTTGTG GCGG-3′ with SacI.

We used NheI and KpnI restriction endonucleases to cleave the viscous end of the PCR amplified fragment, and then purified the amplified fragment with DNA purification kit. Then, the vector plasmid pEGFP-C1 of E. coli DH5 alpha was amplified, the fragments were separated by electrophoresis, and the fragments were extracted and purified by OMEGA Gel Extraction Kit (Omega Bio-Tek, Norcross, GA, USA) and Plasmid DNA Purification Kit (BioVision, Milpitas, CA, USA). Finally, GFAP protein and fluorescent protein probe were linked to pEGFP-C1 and transformed into E. coli culture. Then, we cloned GFAP and incorporated it at each side of cpstFRET to create pCMV-GFAP-cpst-GFAP (GcpG). The pCMV-tubulinα-cpst-tubulin-β (TcpT) was created as well, following the same method. Positive clonal probe was obtained by G418-selection. Moreover, the plasmids encoding Actin-cpst-Actin (AcpA) were obtained from Frederick Sachs and Fanjie Meng (University at Buffalo, Buffalo, New York, USA).

We used an E.Z.N.A.™ Endo-free Plasmid DNA Mini Kit II (Omega Bio-Tek, Norcross, GA, USA) to extract single-colony plasmids according to manufacturer instructions. The integrity of all expression constructs was confirmed by DNA sequencing. Plasmids encoding the FRET sensor were transfected into U87 cells with FuGENE® 6 Transfection Reagent (Roche Diagnostics, Basel, Switzerland) and Opti-MEM™ media (Invitrogen, Carlsbad, CA, USA) according to manufacturer instructions. The transfection efficiency was about 60%. Transfected U87 cells were sorted using a MoFlo™ XDP Cell Sorter with Summit 5.3 software (Beckman Coulter, Fullerton, CA, USA), for which a cyan (458 nm) laser and 447/60 bandpass filter and yellow (514 nm) laser and 580/23 bandpass filter were employed. Cells were sorted when the cyan and yellow emission wavelengths were detected simultaneously. The sorted U87 cells were diluted into single cells and then seeded onto 96-well plates. In all experiments, the sorted single cell lines were trypsinized, and then the cells were incubated with cell culture media for 24–36 h.

2.3. cpstFRET analyses

The dipole angle between donor/eCFP and acceptor/eYFP determined the effectiveness of FRET. Cells were imaged using a confocal microscope (SP5; Leica, Wetzlar, Germany) equipped with a × 63 oil-immersion objective lens. The donor and acceptor were tested by argon lasers at 458 nm and 514 nm, respectively. CFP/FRET ratios were calculated using the equation 1/E = cerulean donor/venus acceptor.

2.4. FRET-AB and FRAP analyses

LAS AF Application Wizard v1.7.0 (Leica) was used for detailed analyses of probes, including live cell acceptor photobleaching FRET (FRET-AB) experiments and fluorescence recovery after photobleaching (FRAP) experiments. We bleached the acceptor in the whole cell and calculated the efficiency of FRET. The recovery curve was used to estimate probe activities.

2.5. Cells area ratio analysis

The cell area was estimated using Image J package 1.48 v (National Institute of Health). CFP/FRET image was converted to the gray-scale image. Based on the pixel distinction between the objects of interest (cells) and the background of objects, area of cell cross section was automatically calculated by the software.

2.6. Calcein fluorescence imaging

Prior to the experiment, cells were mounted in a closed chamber on the stage of an inverted confocal laser scanning microscope (SP5; Leica,

Wetzlar, Germany) in isosmotic, 300 mOsm/kg HEPES, loaded with 10 μM calcein-AM (Molecular Probes, Invitrogen, USA) for 30 min at room temperature, and then washed with HEPES. Fluorescence images were acquired every 60 s with an epifluorescence microscope with a GFP filter. Calcein fluorescence time series were calculated by normalizing calcein fluorescence at each time point (Ft) by the calcein fluorescence at time 0 (F0). Fluorescence intensity in the cell in question was quantified from these data by Image Pro-Plus (Media Cybernetics, Rockville, MD, USA) in the chosen area of interest.

2.7. Measurement of cytoplasmic OP and Count Rate of protein particles

Cell culture medium, HEPES isosmotic solution, and trypsin solution were standardized. Cells were cultivated in 90-mm Petri dishes. When the density was > 95%, drugs were added for a certain duration. Then, specimens were transferred into 1.5-mL microcentrifuge tubes. Ultrasonification (75% amplitude, five times, 5 s) (Sonics and Materials, Connecticut, CT, USA) and ultracentrifugation (21,000 g, 10 min, room temperature) were undertaken. Then, 50 μl of the supernatant solution (cytoplasm) was placed into 0.5-mL test tubes. An Osmomat 3000 Freezing Point Osmometer and 050 Membrane Osmometer (Gonotec, Berlin, Germany) were calibrated thrice before use. Then, cytoplasmic OP was recorded, the supernatant was diluted, and the kilocycles per second (Kcps) of cytoplasmic nanoparticles was detected (Nanosight NS300; Malvern Instruments, Malvern, UK).

2.8. Western blotting

The extracted total proteins were separated by sodium dodecyl sulfate-polyacrylamide gel electrophoresis. Then, the protein bands were transferred to Nitrocellulose filter membranes via wet electrotransfer. Subsequently, the membranes were blocked with 5% skimmed milk in Tris-buffered saline containing 0.1% tween 20 (TBST) at room temperature for 1 h and incubated with primary antibodies, including GFAP, actin-β, tubulin-α, cofilin, stathmin-1, phospho-cofilin (Ser3) and phospho-stathmin-1 (Ser16), at 4 °C overnight. The membranes were then probed with peroxidase-labeled affinity-purified antibodies against rabbit or mouse IgG (H + L) from ImmunoWay (Plano, TX). Target bands were visualized after the addition of Super ECL Detection Reagent Kit from Yeasen (Shanghai, China). Results were normalized to β-tubulin or β-actin levels.

2.9. Immunofluorescence

Astrocytes were fixed with 4% paraformaldehyde. Astrocytes were incubated with blocking buffer (0.1% Triton X-100, 1% bovine serum albumin) for 45 min at 37 °C, and with antibodies overnight at 4 °C. Washing with PBS was followed by addition of goat anti-mouse-FITC secondary antibody (1:200 dilution), goat anti-mouse-TRITC secondary antibody (1:200), and FITC-phalloidin and incubation for one hour at room temperature. Finally, 4′,6-diamidino-2-phenylindole (DAPI) was used to stain nuclei. Fluorescent cells were examined with an inverted fluorescence microscope to appraise cell frameworks.

2.10. Animals

All procedures were conducted according to guidelines established by the National Institutes of Health (Bethesda, MD, USA). The study protocol was approved by the Research Animal Care Committee of Nanjing University of Chinese Medicine.

Adult male Sprague-Dawley rats (240–260 g) were obtained from the Model Animal Research Center of Nanjing University of Chinese Medicine (Nanjing, China) and housed in a 12 h light/dark cycle room. All rats were allowed free access to food and water under conditions of controlled humidity and temperature (24 ± 0.5 °C).

2.11. Water content in rat brains

The water content of rat brains was measured using standard wet-dry methods. Rats were placed in a stereotaxic frame after inhaled anesthesia with a mixture of anesthetic gases isoflurane (1.5–2.0%) and oxygen. The needle of a 10-μl Hamilton syringe (Shanghai Gaoge Industry & Trade Co., Ltd., Shanghai, China) was inserted into the right lateral ventricle through a burr hole using the following coordinates: right side of a sagittal suture (3.5 mm) and coronal suture (2 mm). Glutamate (1.67 mol/L) was injected into the right lateral ventricles at a rate of 0.5 μl/min with a 10-μl Hamilton syringe. In the meantime, drugs were injected via the intraperitoneal route. The body temperature was controlled at 37.0 ± 0.5 °C throughout the surgery using a heating pad. Then rats were killed by decapitation after 4 h. The brainstem was discarded, while the tissue of ipsilateral cortex, the contralateral cortex, and the cerebellum was harvested. The wet weight of each cortical tissue was measured, and then dried for 72 h at 80 °C and the dry weight determined. Water content was calculated as a percentage using the formula:

Water content = (wet weight − dry weight)/wet weight × 100%

2.12. IHC analyses and H&E staining

Brains were fixed in 4% paraformaldehyde in PBS over 24 h at 4 °C and then dehydrated in a graded series of alcohol solutions by xylene and embedded in paraffin. Brain tissues were cut at 5 μm, stained for expression of p-cofilin and p-stathmin-1 by H&E, and viewed under a microscope (CM3050 S; Leica). Images were captured per slide at 40 × magnification using a microscope (DMi8; Leica). Semi-quantitative analyses of IHC images was conducted using Image Pro-Plus v6.0, from which integral optical density (IOD) and area data were collected. Then, the average optical density was calculated as IOD/area, which represented the staining intensity.

2.13. Statistical analyses

The YFP/CFP ratio was calculated using ImageJ (San Diego, CA, USA). The FRET value in each subcellular region was measured for each cell and then averaged over multiple cells. Images were pseudo-colored using the 16-color map in ImageJ. Data were presented as mean ± SEM. One-way ANOVA with the least significant difference test was used to determine statistical significance and P < 0.05 was considered significant. Each experiment was repeated at least three times, > 10 cells were imaged, and each condition was analyzed. The R-value of U87 cells is presented as the pixel count distribution from > 9 cells.

3. Results

3.1. The probe could be used to detect cell swelling under extracellular stress

Astrocyte swelling is an integral component of cytotoxic brain edema and can be caused by water movement into intracellular compartments [34,35]. We employed the probe to explore the intracellular function of GFAP in U87 cell swelling. The probe demonstrated resonant angle twisting toward a perpendicular configuration through a reduction in energy transfer. The periphery of the GFAP backbone was embedded with a FRET module (Fig. 1A). The GFAP probe was transfected into U87 cells, followed by cell sorting with fluorescence (Fig. S1A). The FRET signals of GFAP tension in astrocytes under isotonic conditions was detected optically using laser confocal Z-axis scavenging (Fig. 1B, row one) and the 16-bit images were saved (Fig. 1B, row two). Results suggested that GFAP tension rarely changed from the bottom layer to the top layer. The acceptor fluorescence (eYFP) was decreased dramatically upon acceptor photobleaching (AB). Concurrently, the
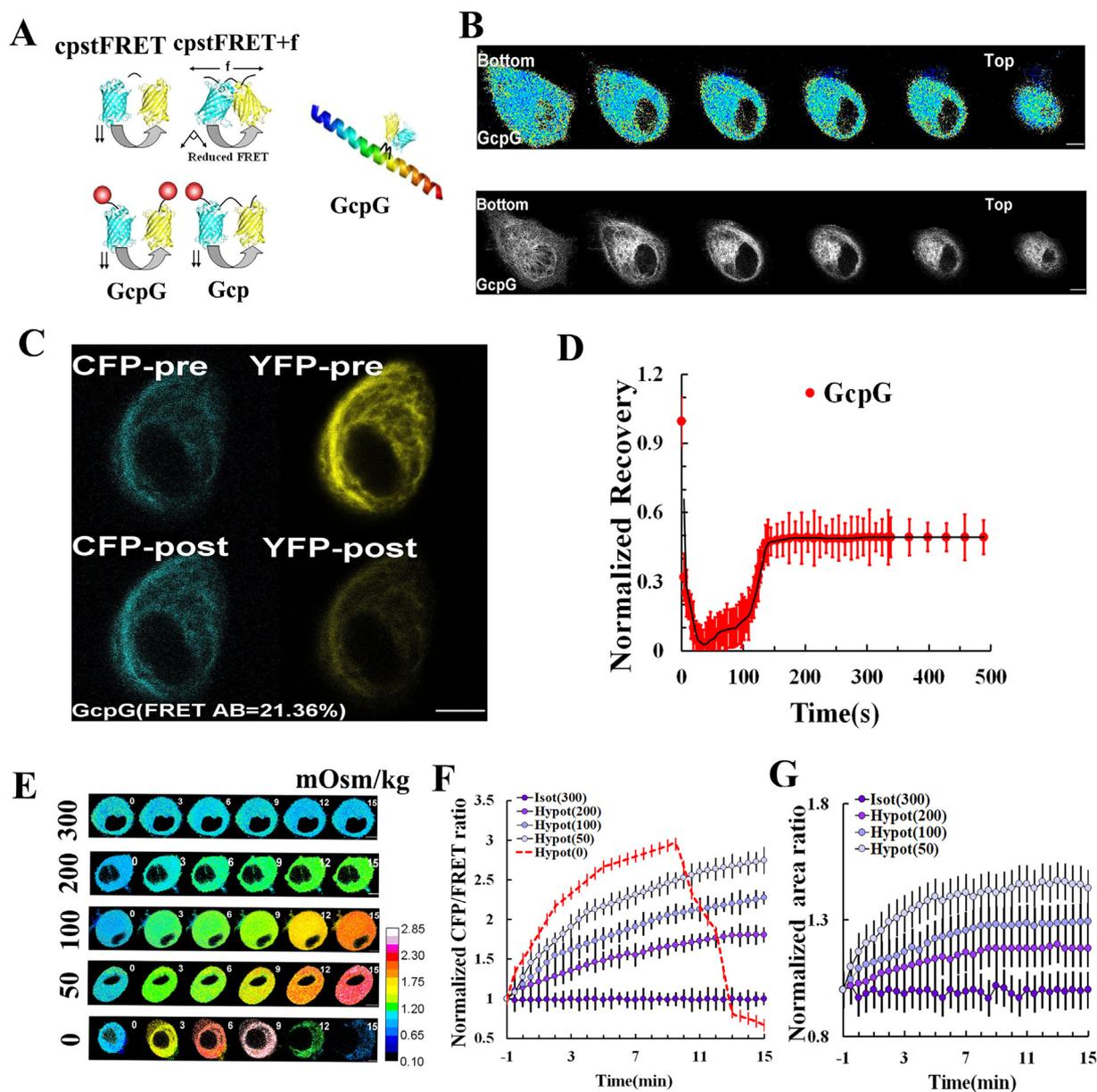
Fig. 1. Analyses of the construction and efficacy of the GFAP probe and its application to U87 cell swelling under different hypoisotonic pressures. (A) U87 cells with the GFAP probe were tested using 458-nm and 514-nm argon lasers. The GFAP probe comprised pCMV-GFAP- cpCerulean-7aa-cpVenus (cpstFRET)-GFAP (GcpG). CpVenus was parallel to cpCerulean at resting cells. When the external force across cpstFRET generated a certain angle, the Förster resonance energy transfer (FRET) efficiency was reduced (f: external force). (B) Representative Three-dimensional images of GcpG tension (n = 6). The top of GcpG had as much tension as the bottom. The image was processed and pseudocolored by the 16-color map of ImageJ. (C) FRET acceptor photobleaching (AB) tested the reliability of the GcpG probe. (D) The intracellular mobility of the GcpG probe was examined using fluorescence recovery after photobleaching. The normalized average fluorescence recovery of GcpG vs. time (500 s) was calculated (n = 8). The fluorescence recovery ratio was noted. (E) U87 cells were treated with five concentrations of HEPES buffer, thus generating hypoosmotic pressures (300, 250, 200, 100, 0 mOsm/kg). (F) Normalized CFP/FRET signals corresponding to GFAP tension vs. time under the five hypotonic conditions. The calibration bar was set from 0.10 to 2.85. (G) Normalized area ratio under five osmotic pressures vs. time. Average of ≥ 5 experiments ± stand error of the mean (SEM). (Scale bar = 20 μm.).

donor fluorescence (eCFP) was increased due to the unacceptable energy transfer from donor to acceptor after photobleaching (GcpG FRET AB = 21.36%; Fig. 1C). Fluorescence recovery after photobleaching (FRAP) was measured and showed that the recovery rate for GFAP was 48.52% after 500 s (Fig. 1D). The molecular weight of GcpG, Actin-cpst-Actin (AcpA), and Tubulinα-cpst-Tubulinβ (TcpT) tension probes were determined (Fig. S1B and S1C). As for the negative control, Gcp, the FRET index was very high compared with the tension probe (Fig. S1 D-F). All the results showed that the genetically encoded FRET-based tension probes were established and effective.

The outward tension induced by hypo-OP results in the "pulling" of cytoskeletal filaments, which is involved in cell swelling, increased volume, and altered cytoskeletal structural tension [36]. To measure GFAP tension during cell swelling, we exposed U87 cells to hypo-osmotic stress through switching the 300 mOsm/kg bath (isotonic HEPES buffer) to hypo-osmotic conditions, of which follows 200, 100, 50, and 0 (pure water) mOsm/kg (Fig. 1E). Cells started to swell with the reduced osmotic pressure (Fig. 1G), at the same time the GFAP tension increased gradually (Fig. 1F). Also, cells disintegrated along with exudation of cytoplasm when OP decreased to 0 mOsm/kg, and GFAP tension declined rapidly. These data suggested that increased GFAP tension was involved in cell swelling and cell volume enlargement.
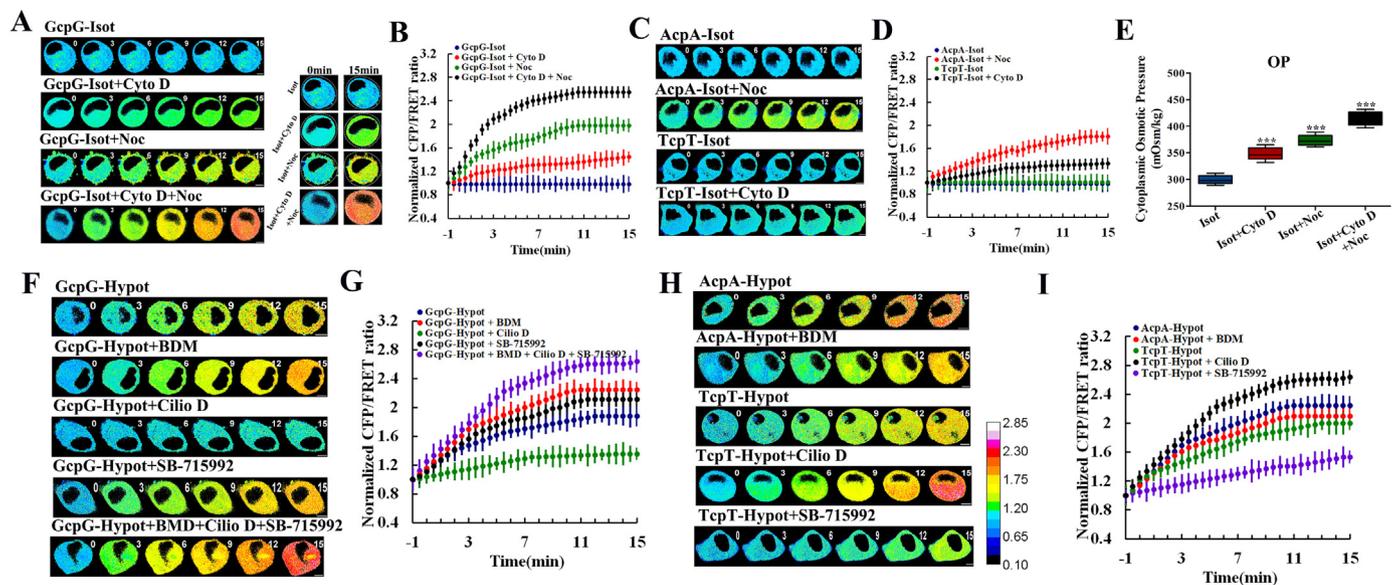
Fig. 2. GFAP tension changes in U87 cells produced by suffering hypotonic pressure and the mechanism of action. (A) Representative images of normalized CFP/FRET ratios of GFAP tension subjected to isotonic treatment alone (row 1), with cytochalasin D (row 2,10 μM), nocodazole (row 3, 100 μM), or both agents (row 4). Cell volumes were determined at the initial and final times (right panel). (C) MF and MT tension after being subjected to isotonic treatment alone (row 1 and 3), MF with nocodazole (row 2) and MT with cytochalasin D (row 4). (F) GFAP tension in response to hypotonic stimuli alone (row 1), with 2,3-Butanedione monoxime (row 2, 10 mM), ciliobrevin D (row 3, 20 μM), SB-715992 (row 4, 1 μM), or both agents (row 5). (H) MF and MT tension in response to hypertonic stimulation alone (row 1 and 3), MF with 2,3-Butanedione monoxime (row 2), MT with Cilio D (row 4) or MT with SB-715992 (row 5). (B, D, G, and I) Mean values of normalized CFP/FRET ratios in GFAP (2 A and 2 F), MF and MT (2 C and 2 H) under isotonic or hypo-osmotic pressure responses to different reagents. The dark-blue calibration bar indicates the smallest tension (0.10), whereas red indicates the largest tension (2.85). (E) The osmotic pressure of cytoplasm in U87 cells in response to isosmotic pressure and with cytochalasin D, nocodazole, or both agents. Average of ≥ 5 experiments ± SEM. ***p < 0.001. (Scale bar = 20 μm.).

Therefore, our probe could be used to detect astrocyte swelling.

3.2. OP, MF, and MT forces are involved in regulation of GFAP tension

First, we explored the role of MF and MT forces in mediating GFAP tension and the relationship between cellular morphology and skeletal tension. Cytochalasin D (Cyto D) (10 μM) and nocodazole (Noc) (100 μM) were used to depolymerize MFs and MTs, respectively. MF depolymerization induced a relative increase of GFAP and MT tensions compared with isotonic treatment. MT depolymerization aggrandized GFAP and MF tensions. Co-treatment of cytochalasin D and nocodazole increased GFAP tension enormously, and U87 cells expanded slightly (Fig. 2A–D).

Depolymerization of MFs, MTs or both could increase OP markedly (Fig. 2E). Experiments using Zetasizer Nano instruments suggested that nanoparticles of diameter < 10 nm were produced after depolymerization of MFs and MTs within 15 min. (Fig. S3B–D). We also test the control cells which cultured in the isotonic environments using the same methods. The nanoparticle size experiments showed that there was no obvious sub-100 nm granule generating (Fig. S3A). The value of osmotic pressure of the control cells was in close proximity to 300 mOsm/kg (Fig. 2E), which accorded with the average magnitude of cytoplasm OP ever reported [37]. Besides, the colloid OP, as determined by a colloidal osmometer, was increased after 2-h co-treatment with depolymerizing agents (Fig. S3E). This result suggested that depolymerization of MFs and MTs could increase the GFAP tension and involved in cell expansion, while protein nanoparticle produced from skeleton depolymerization could generate colloid OP.

Inhibitors of myosin, dynein, and kinesin were employed to ascertain if astrocyte swelling was related to cytoskeletal molecular motors; the inhibitors were 2,3-Butanedione monoxime (BDM) (10 mM), ciliobrevin D (Cilio D) (20 μM), and ispinesib (SB-715992) (1 μM), respectively. MF, MT, and GFAP tension increased as cells swelled after hypo-osmotic stimulation (Fig. 2F–I). GFAP tension increased and MF tension decreased when myosin was inhibited. Dynein inhibition could reduce

GFAP tension and increase MT tension. However, kinesin inhibition resulted in the opposite result. Inhibition of dynamic molecules on MFs and MTs could increase GFAP tension more distinctly (Fig. 2F–I). These results suggested that the inward forces of MFs and MTs antagonized GFAP tension in response to outward OP in swelling U87 cells and that the intracellular mechanical system had an essential role in cell swelling.

3.3. Construction of a model of astrocyte swelling; GFAP tension participated in glutamate-induced astrocyte swelling

To investigate the role of cytoskeletal structural tension during astrocyte swelling, we constructed three U87 cells models treated by glutamate (Glu) (2 mM), caffeine (5 mM), and NaN$_3$ (20 mM) respectively (Fig. 3A).

When stimulated with glutamate, GFAP tension increased markedly within 15 min. Glutamate can elicit Ca^{2+} influx and activation of molecular motors [38]. However, the Ca^{2+} level in cytoplasm increased in Caffeine-treated U87 cells, but the cell volume and GFAP tension did not change evidently. After depletion of cellular energy, vesicles were observed in cells [39], but GFAP tension and cellular area decreased (Fig. 3B). In addition, the decrease of cell area in the NaN3 treatment samples was statistically significant compared to the control (p = 0.0316, Fig. 3C). The cytoplasmic OP of astrocytes was also measured in the three models at different time points within 24 h (Fig. 3D). Glutamate could change the intracellular OP of astrocytes clearly, and reached a peak at 12 h. Changes in cell volume were monitored continuously with calcein (a self-quenching dye that exhibits fluorescence that is proportional to the cell volume). Glutamate stimulation resulted in a "piecemeal" increase in calcein fluorescence during 15 min (Fig. 3E and F). Overall, these results showed that glutamate could increase the volume of U87 cells. Hence, it could be used to construct a model of cell swelling in vitro.

To explore the influence exerted on the cytoskeleton under the three models, the intracellular structural features of the cytoskeleton were
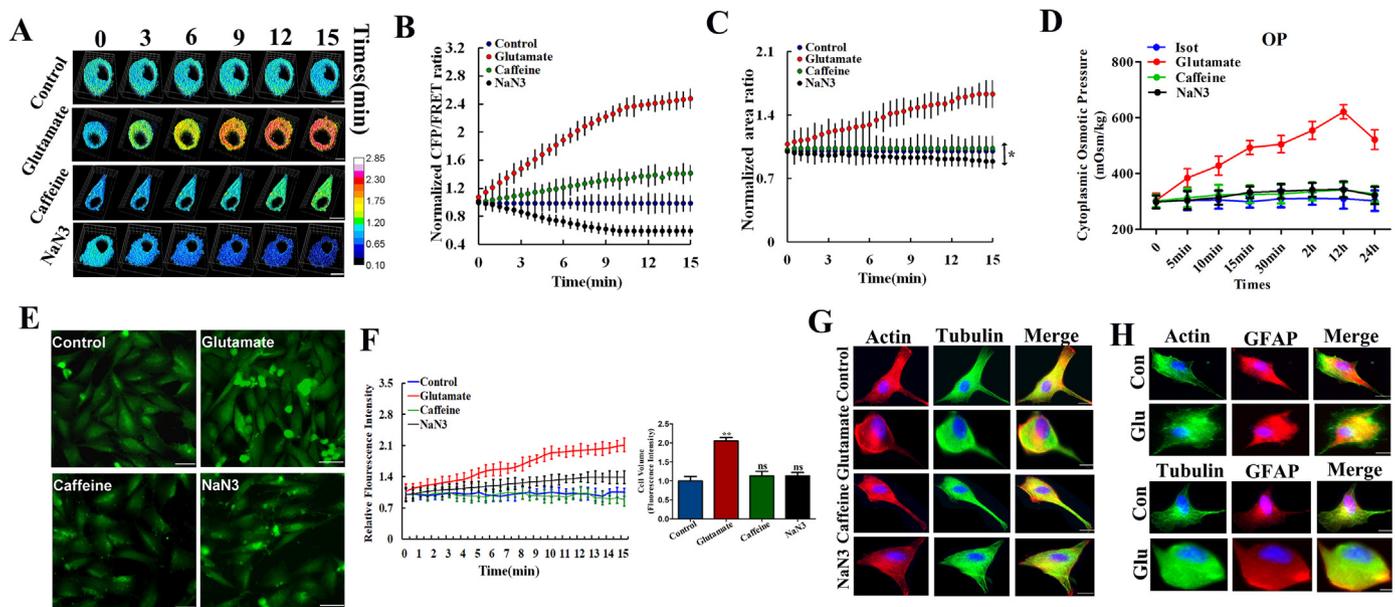
Fig. 3. Comparison of GFAP tension, surface area, cytoplasm osmotic pressure, cell volume, and cytoskeleton structure in different cellular models. (A) U87 cells expressed the GFAP probe. Representative three-dimensional reconstructions of the control (row 1) or treatment with glutamate (row 2, 2 mM), caffeine (row 3, 5 mM) or NaN3 (row 4, 20 mM). (B) Mean CFP/FRET ratios over the whole cell were expressed by measuring the relative increase compared with the reference value, which was averaged over 15 min. Blue, red, green, and black lines denote results for the control, cytotoxic edema, calcium overload, and energy-depletion models, respectively. The calibration bar was set from 0.10 to 2.85. (C) Normalized area ratio in control and three models vs. time. The cell area in the NaN3 treatment (15 min) samples marked with * is significantly decreased (p = 0.0316) than the corresponding measurement in the control samples as determined by t-test. (D) Cytoplasm osmotic pressure of U87 cells in response to chemical stimuli vs. time. (E) calcein-fluorescence micrographs of U87 cells at 15 min in experiments with different chemical stimuli. (F) Traces of relative calcein fluorescence intensity (Ft/F0) in U87 cells showing comparisons with control (blue), glutamate (red), caffeine (green) and NaN3 (black). (G) Control, glutamate-, caffeine-, and nNaN3-treated U87 cell monolayers were stained for β-actin (TRITC) and α-tubulin (FITC). Images were generated from confocal laser microscopy after immunofluorescence staining. (H) U87 cells were transfected with tension probes, and confocal laser microscopy analyzed immunofluorescence staining for β-actin (FITC), α-tubulin (FITC), and GFAP (TRITC) in control or the astrocyte-edema model. Average of ≥ 5 experiments ± SEM. ns, p > 0.05, **p < 0.01, ***p < 0.001. (Scale bar = 20 μm.).

analyzed. Confocal microscopy was employed to examine the cytoskeleton, among which actin was assessed with tetramethylrhodamine-isothiocyanate (TRITC) staining, and tubulin was labeled with fluorescein isothiocyanate (FITC) in U87 cells. Incidentally, morphologic changes in the cytoskeleton in glutamate-model cells were observed (Fig. 3G). Experiments on nanoparticle diameters demonstrated that the intracellular distribution of nanoparticles after glutamate stimulation was similar to that obtained using depolymerizing agents, and that colloid OP was increased too (Fig. 6B; Fig. S3D and S3E).

To explore if the transfected probes affected cell structure, we monitored the cytoskeletal structure in astrocytes transfected with different tension probes. MFs, MTs, and GFAP remained unchanged when transfected with the three tension probes, whereas MFs and MTs underwent slight deformation after glutamate treatment (Fig. 3H).

To summarize, glutamate stimulation could cause an increase in the total OP, colloid OP, cell volume, and astrocytic swelling. Cytotoxic brain edema is closely related to cytoplasmic colloid OP and cytoskeletal changes, and we hypothesized that the depolymerization of MFs and MTs occurred in glutamate-induced cell swelling.

3.4. Stabilization of the structure of MTs and MFs antagonized the astrocyte swelling induced by glutamate

Glutamate-induced astrocyte swelling is thought to be closely associated with cytoskeletal rearrangement [40]. To assess the roles of the cytoskeleton in U87 cell swelling, we employed the MF stabilizer jasplakinolide (JK) (10 μM) and MT stabilizer taxol (TAX) (15 μM).

We found that jasplakinolide treatment could reduce GFAP tension and cell edema compared with the model. Similarly, taxol treatment also reduced GFAP tension and the relative fluorescence intensity of calcein. Upon co-treatment with jasplakinolide and taxol, the decrease

in GFAP tension and edema was more apparent (Fig. 4A, B, D, and E). Studies (Figs. 1–3) have suggested that the cytoskeleton and OP are closely related, so stabilizers of MFs and MTs were employed to observe OP changes during U87 cell swelling. The value of OP decreased in the jasplakinolide, taxol or co-treatment group (Fig. 4C). Meanwhile, nanoparticles of diameter 1–10 nm were eliminated, and the cytoplasmic OP and colloid OP decreased (Fig. 6C; Fig. S3E). These results confirmed that glutamate-induced U87 cell swelling was caused by the increased cytoplasmic OP, colloid OP, cytoskeleton depolymerization, and nanoparticle production. Meanwhile, stabilization of MFs and MTs could recover cytoplasmic OP (particularly the colloid OP) and reduce cell swelling.

Inhibitors of myosin, dynein, and kinesin were employed to ascertain if motor molecules had effects on cell swelling. Inhibition of myosin could increase GFAP tension and decrease MF tension (Fig. 4F and H). GFAP tension was weakened and MT tension increased when dynein was inhibited, but the opposite results were observed when kinesin was inhibited. GFAP tension increased more significantly when all the molecular motors on MFs and MTs were inhibited simultaneously (Fig. 4F–I). However, cell edema was not reduced upon treatment with molecular-motor inhibitors within 15 min (Fig. 4J and K).

In summary, OP cooperated with inward MF and MT tension and had essential roles in U87 cell swelling. Molecular motors could regulate cytoskeletal structural tensions, whereas inhibiting their function did not help to reduce cell edema.

3.5. Mechanisms underlying depolymerization of MFs and MTs in response to glutamate stimulation

Astrocyte swelling has been demonstrated to be related to the disaggregation of the cytoskeleton, but this mechanism must be studied
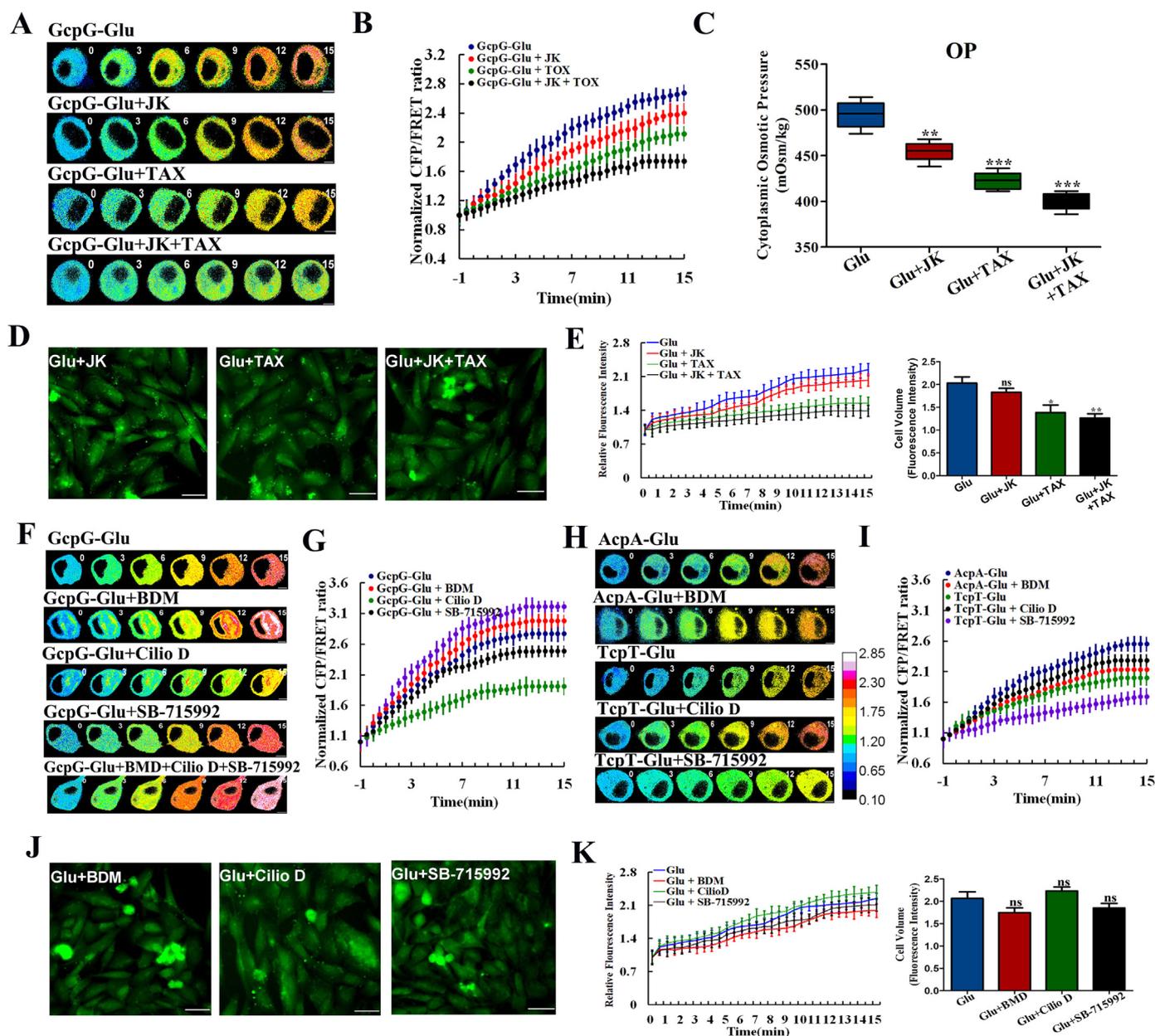
Fig. 4. The temporal curve of GFAP, MF, and MT tensions in the development of cell swelling and their interactions. (A) GFAP tension was analyzed in the cytotoxic-edema model of U87 cells subjected to glutamate alone (row 1), with jasplakinolide (row 2, 10 μM), taxol (row 3, 15 μM), or both agents (row 4). (F) GFAP tension was analyzed in U87 cells subjected to glutamate alone (row 1), with 2,3-Butanedione monoxime (row 2), Cilio D (row 3), SB-715992 (row 4) or all agents (row 5). (H) MF and MT tension after treatment with glutamate (row 1 and 3), MF with 2,3-Butanedione monoxime (row 2), MT with Cilio D (row 4) or MT with SB-715992 (row 5) vs. time. The calibration bar was set from 0.10 to 2.85. (B, G, and I) Mean values of normalized CFP/FRET ratios in GFAP, MF, and MT. (C) Cytoplasm osmotic pressure of U87 cells in response to glutamate, with jasplakinolide, taxol or both agents. (D and J) Calcein-fluorescence micrographs of U87 cells at 15 min in experiments involving treatment with MF and MT stabilizers or molecular-motor inhibitors. (E and K) Traces of relative calcein fluorescence intensity (Ft/F0) in U87 cells showing comparisons with glutamate (blue), jasplakinolide or 2,3-Butanedione monoxime (red), taxol or Cilio D (green) and both agents or SB-715992 (black). Average of ≥ 5 experiments ± SEM. ns $p > 0.05$, **$p < 0.01$, ***$p < 0.001$. (Scale bar = 20 μm.).

further. Cofilin and stathmin-1 are depolymerization factors for MF and MT, respectively [41,42]. We found that glutamate activation was correlated directly with the dephosphorylation of p-cofilin and p-stathmin (Fig. 5A–D). Moreover, significant activation of cofilin and stathmin was also detected by immunohistochemical (IHC) staining in vivo (Fig. 5E and F). These data suggested that glutamate could lead to the depolymerization of MFs and MTs through activation of cofilin and stathmin-1.

To explore the signaling pathways involved in this process, we used a calcium antagonist (nimodipine (NMDP), 30 μM), Shingshot (SSH) inhibitor (sennoside A (Sen), 100 μM), and Protein phosphatase 2a

(PP2A) inhibitor (cantharidin (Can), 2 μM). Inhibition of calcium signaling and SSH could recover the phosphorylation levels of cofilin, while inhibition of calcium signaling and PP2A could recover stathmin-1 phosphorylation (Fig. 5G–J). Similar results were observed in IHC staining in vivo (Fig. 5K and L).

To summarize, activation of calcium signaling, SSH, and PP2A is involved in depolymerization of MFs or MTs during glutamate-induced cytotoxic edema. Hence, the hypothesis that inhibition of calcium signaling, SSH or PP2A could reduce OP and ease brain edema merited further research.
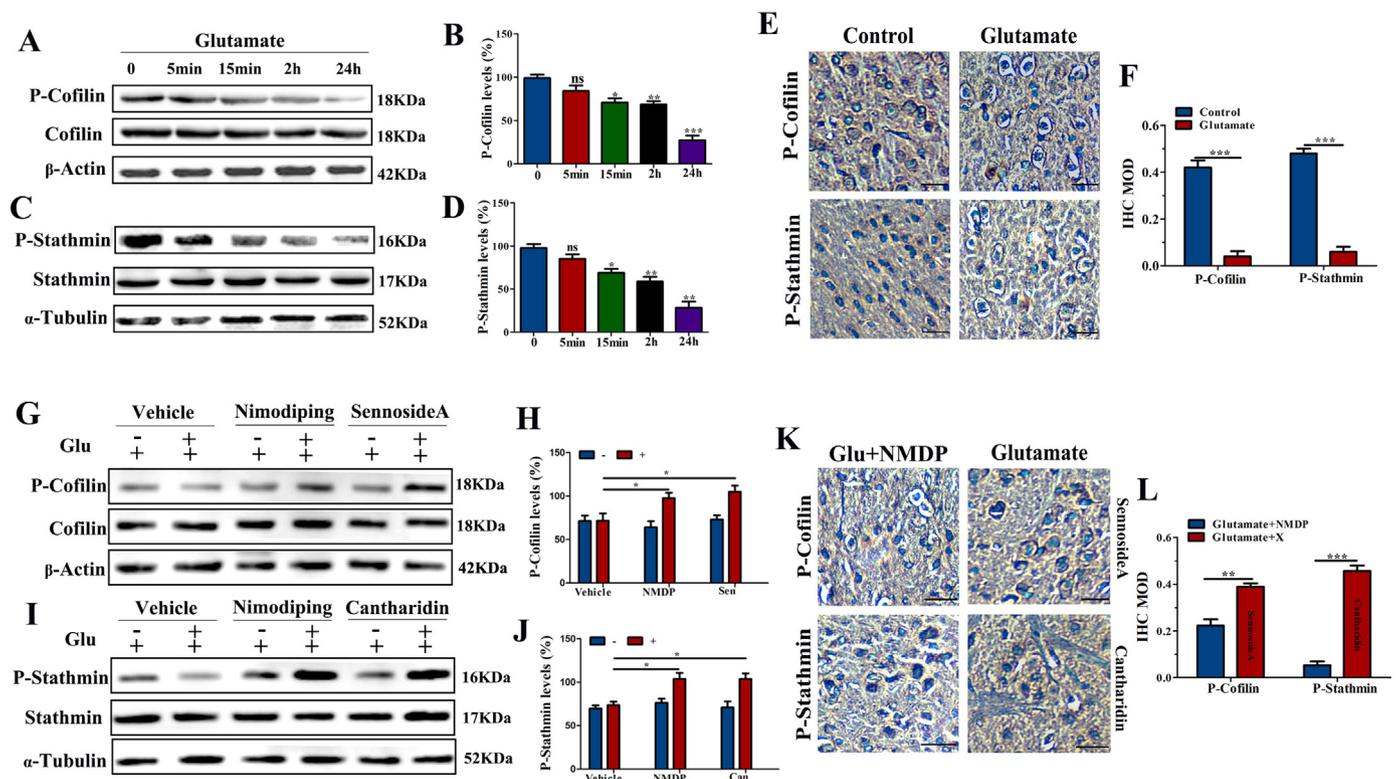
Fig. 5. MF- and MT-related proteins could participate in cell swelling in response to glutamate stimulation. (A and C) Glutamate-induced dephosphorylation of cofilin and stathmin. P-cofilin, cofilin, β-Actin, p-stathmin, stathmin, and α-tubulin were detected by immunoblotting at the indicated times. (G and I) Glutamate-induced dephosphorylation of cofilin and stathmin. P-cofilin, cofilin, and β-Actin were detected by immunoblotting in the vehicle, nimodipine (30 μM), and sennoside-A (100 μM) treatment groups. P-stathmin, stathmin, and α-tubulin were detected by immunoblotting in the vehicle, nimodipine, and cantharidin (2 μM) treatment groups. (B and D) Relative p-cofilin or p-stathmin levels, with the value in non-treated cells taken as 100%. (H and J) Relative p-cofilin or p-stathmin levels in the absence (−) or presence (+) of vehicle, sennoside-A or cantharidin. (E and K) IHC analyses of brain tissue subjected to control, glutamate, glutamate with sennoside-A or cantharidin stimulation. Cytoplasm was stained with p-cofilin or p-stathmin antibodies (brown). (F and L) Semi-quantitative analyses of IHC staining by comparison of average optical density among the groups (average of three experiments ± SEM); ns, p > 0.05, *p < 0.005, **p < 0.01, ***p < 0.001. (Scale bar = 20 μm.).

3.6. Certain drugs reduced the levels of intracellular ions or protein nanoparticles-induced OP during astrocyte swelling

β-actin and α/β-tubulin are abundant in astrocytes. Typically, β-actin and α/β-tubulin can help to construct the cytoskeletal structure to maintain the morphology and function of cells by polymerization [43]. Under normal conditions, the size distribution of cytoplasmic particles was > 100 nm (Fig. 6A). Under the action of depolymerizing agents and glutamate treatment, monomers of actin and tubulin or macromolecular polymers were produced, the composition and magnitude of cytoplasmic OP changed. Here, we termed the cytoplasmic OP changes induced by these granules as protein nanoparticles-induced osmotic pressure (PN-OP) but not colloid OP in view of the theory of Van't Hoff effect and Gibbs-Donnan equilibrium [37,44,45], which would be illustrated detailedly in the discussion part. A standard curve was generated using different concentrations of depolymerization agents to produce different OP values after 2-h treatments (Fig. 6D). The formula for the PN-OP was: $\triangle$PN-OP $= 0.93 \times - 218.69$ ($R^2 = 0.97$). The results suggest that production of protein nanoparticles and OP increment has a linear relationship significantly.

To explore molecular mechanisms underlying OP in swollen U87 cells, we screened the impact of different drugs and their effective concentrations on the ion osmotic pressure (IOP) and PN-OP on swelling cells after two hours treatment by glutamate. The optimum level of the SSH inhibitor sennoside A was discovered to be 100 μM (Fig. 6E). PP2A inhibitor cantharidin (2 μM) could reduce OP more effectively (Fig. 6F). Nimodipine is a Ca^{2+}-channel blocker that can penetrate the blood-brain barrier readily [46]. Nimodipine could decrease OP at

30 μM effectively (Fig. 6G). Cinepazide maleate (CM) is a Ca^{2+}-channel blocker that can improve brain metabolism by increasing blood flow in cerebral blood vessels. Cinepazide maleate worked best at 10 μM (Fig. 6I). Cinepazide maleate can inhibit p-stathmin dephosphorylation by inhibiting Ca^{2+}-dependent PP2B release and reduce Ca^{2+}-induced toxicity [47]. Verapamil (Verap) can attenuate Ca^{2+} inflow, but its effect in astrocytes was not distinct (Fig. S4D). The ROCK inhibitors dihydrochloride (Y-27632) and fasudil (HA-1077) inhibited profilin-1 phosphorylation and promoted MF polymerization, whereas Y-27632 was more effective than HA-1077 (Fig. S4A and S4B). Edaravone (ED) is a commonly used brain-protective agent and acts as a free-radical scavenger [48]. The optimal concentration of edaravone was 50 μM (Fig. 6H). Oxiracetam (Oxira) is also a commonly used neuroprotective drug for brain injury, but its effect was suboptimal (Fig. S4C). Tamoxifen (Tam) inhibits volume-regulated anion channels and reduces Cl$^-$ resorption [49]. Tamoxifen could not attenuate OP effectively (Fig. S4E). Blockade of Na-K-Cl cotransporter with bumetanide (Bum) prevents uptake of Na$^+$, K$^+$, and Cl$^-$ in neural cells, but OP was reduced only slightly (Fig. S4F).

Next, drug-combination experiments were conducted based on the concentrations of single drugs that elicited the optimal effect (Fig. 6H and I). The most effective combination of drugs was sennoside A + cantharidin + nimodipine + edaravone + cinepazide maleate ($\triangle$PN-OP decreased by 95.19 ± 19.34 mOsm/kg, and $\triangle$IOP decreased by 64.99 ± 17.68 mOsm/kg). Also, we found that the efficacy of the cytoskeleton stabilizers jasplakinolide and taxol was limited compared with the sennoside A + cantharidin + nimodipine + edaravone group (Fig. S4H).
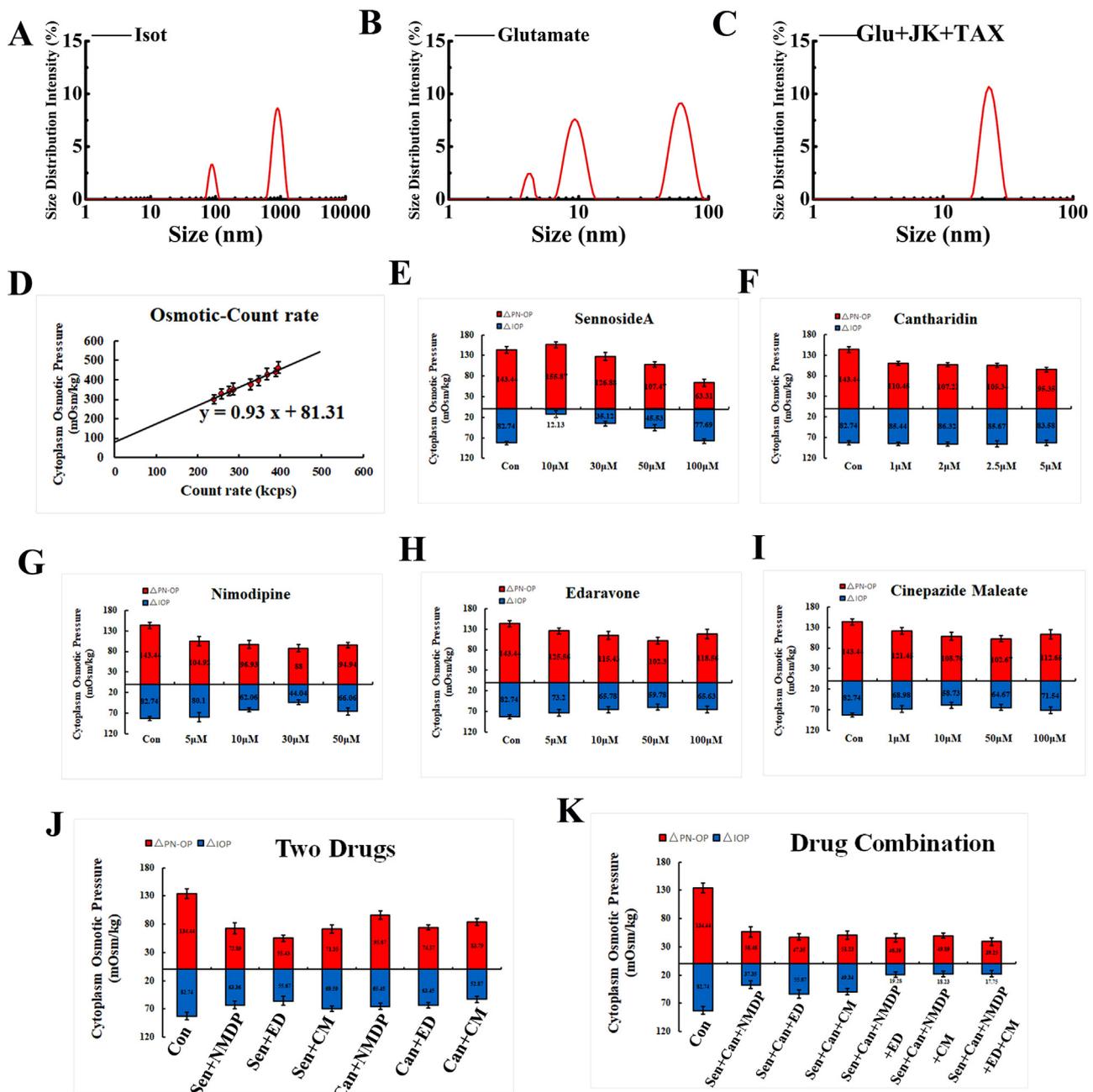
Fig. 6. Drug screening for lowering cytoplasm ion or protein nanoparticles-induced osmotic pressure. (A-C) Size distribution of protein granules in the cytoplasm was detected in response to isosmotic stimulation, glutamate stimulation, and cytoskeleton stabilizers. (D) Under the isotonic condition, the curve of the relationship between the count rate (Kcps) and osmotic pressure (mOsm/kg) induced by MF and MT depolymerization agents with different concentration is shown. The histograms show the values of protein nanoparticles-induced osmotic pressure (red) and ion osmotic pressure (blue) induced by the single-drug administration. (E) Administration of the SSH inhibitor sennoside-A at 10, 30, 50, and 100 μM alone. (F) Administration of the PP2A inhibitor cantharidin at 1, 2, 2.5, and 5 μM alone. (G) Administration of the calcium antagonist nimodipine at 5, 10, 30, and 50 μM alone. (H and I) Commonly used clinical drugs for the treatment of brain injury. The concentration of edaravone and cinepzaie maleate was 5, 10, 50, 100 and 1, 10, 50, 100 μM, respectively. Results of the combined use of the drugs stated above. Average of ≥ 3 experiments $\pm$ SEM.

To summarize, the cytoskeletal depolymerization of astrocytes induced by glutamate could result in the production of protein granules, and then generate protein nanoparticles-induced osmotic pressure (PN-OP). Administration of Ca^{2+}-channel inhibitors, neuroprotective agents, combined with specific drugs, and agents that inhibit the depolymerization factors of MFs and MTs reduce the ion OP and PN-OP of U87 cells effectively in vitro.

3.7. Effective drug combinations reduced GFAP tension and cell volume during astrocyte swelling

We showed that single drugs (sennoside A, cantharidin, nimodipine, edaravone, and cinepazide maleate) and their combinations were effective in reducing cytoplasmic OP. Meanwhile, their influences on GFAP tension during cell swelling were observed on U87 cells (Fig. 7A–D). The five drugs stated above given alone could reduce GFAP tension, while combinations of these drugs were more effective. Measurement of the intensity of calcein fluorescence confirmed that a
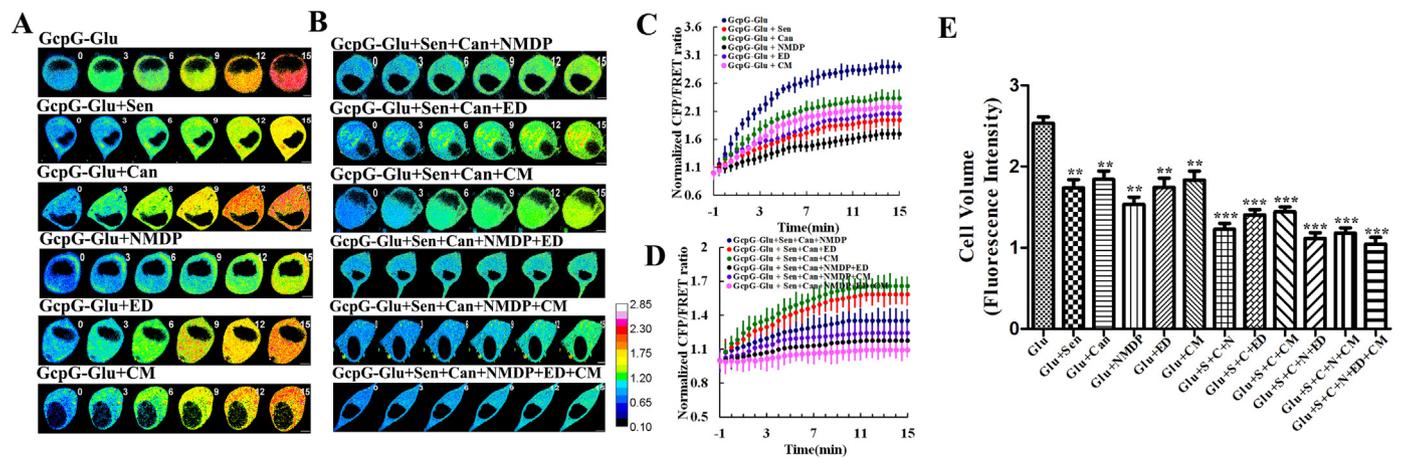
Fig. 7. GFAP tension and osmotic pressure reduced by effective drugs or their combinations in response to Glu stimuli. (A) Representative images of normalized CFP/FRET ratios of GFAP tension after subjection to glutamate alone (row 1), with sennoside-A (row 2), cantharidin (row 3), nimodipine (row 4), edaravone (row 5), or cinepazide maleate (row 6). (B) Representative images of normalized CFP/FRET ratios of GFAP tension after subjection to glutamate treatment with sennoside-A, cantharidin, nimodipine (row 1), with sennoside-A, cantharidin, edaravone (row 2), with sennoside-A, cantharidin, cinepazide maleate (row 3), with sennoside-A, cantharidin, nimodipine, edaravone (row 4), with sennoside-A, cantharidin, nimodipine, cinepazide maleate (row 5), and with sennoside-A, cantharidin, nimodipine, edaravone, cinepazide maleate (row 6). The calibration bar was set from 0.10 to 2.85. (C and D) Normalized CFP/FRET signals of GFAP in the astrocyte-edema model with the same treatment as 7(A) and 7(B). (E) The relative calcein-fluorescence intensity in U87 cells compared with the effects of single drugs and their combined use. Average of ≥ 5 experiments $\pm$ SEM. $**p < 0.01$, $***p < 0.001$. (Scale bar = 20 μm.).

combination of these drugs could alleviate edema in U87 cells (Fig. 7E). Overall, these data suggested that administration of Ca^{2+}-channel inhibitors, neuroprotective agents combined with specific drugs, and agents that inhibit the depolymerization factors of MFs and MTs could attenuate GFAP tension effectively and reduce cell swelling.

3.8. Drug-combination treatment could decrease cytoplasmic OP and reduce cell volume in glutamate-induced astrocyte swelling in primary cultures or in vivo

The potential roles of drug combinations for relieving astrocyte swelling were studied in primary murine astrocytes. Immunofluorescence assays with FITC-labeled actin and tubulin, and TRITC-labeled GFAP was used to identify primary astrocytes (Fig. 8A). The primary glial cells transfected with GFAP probe were applied to detect the effect of combined drugs on cytoskeletal tension. We also detected the changes in cytoplasmic OP and count rate after 2 h of drug action (Fig. 8D). The primary glial cells with transfected GFAP probe were used to detect the effect of drugs combination on cytoskeletal tension. Effective drug combinations could markedly reduce GFAP tension within 15 min (Figs. 8B and 8C). We also detect the changes in cytoplasmic IOP and PN-OP after 2 h of treatment (Fig. 8D). A combination of sennoside A, cantharidin, nimodipine, edaravone, and cinepazide maleate reduced PN-OP (decreased by 86.8 $\pm$ 16.89 mOsm/kg) and IOP (decreased by 59.5 $\pm$ 18.26 mOsm/kg) in primary astrocytes.

To further ascertain the role of drug combinations in astrocyte swelling, we measured the volume of primary astrocytes treated with glutamate for 2 h using the calcein imaging (Figs. 8E and 8F). The optimized drug combination was found to reduce edema by $\approx 65\%$ compared with the control group. Besides, to verify the mechanisms described above in vivo, we employed models of cytotoxic edema on rats. Measurement of the water content of brain tissues suggested that glutamate increased cell edema significantly whereas drug combinations inhibited it (Fig. 8G). Staining with hematoxylin and eosin showed, in the model group, karyopyknosis, hyperchromatic cytoplasm, and triquetrous cells, with surrounding tissues showing fissures. Cells in drug groups had remission of the features mentioned above (Fig. 8H).

Overall, these results suggested that the drug combination could mitigate glutamate-induced edema in primary astrocytes or in vivo

effectively by attenuating cytoplasmic OP, among which PN-OP and IOP were attenuated.

4. Discussion

Cytotoxic astrocyte swelling is a causal effect common to the pathogenesis of brain edema in trauma, ischemia, hemorrhage, inflammation or hepatic encephalopathy [50–53], swelling of the neural cells involves a shift of water from interstitial compartments to intracellular compartments. Water flux is dependent upon its potential in cells [54]. The aqueous influx into astrocyte is based on the premise of intracellular hyper-osmotic pressure or extracellular hypo-osmotic pressure [23,55]. Notably, intracellular tension activity including OP is dependent upon the cytoskeletal structure.

In the present study, we designed a tension sensor module (cpstFRET) that is physically smaller, less invasive, more biocompatible, and with a higher signal-to-noise behavior than linear distance-dependent probes, and its FRET efficiency decreases under pull tension. The dipole orientation-based FRET probes GcpG, AcpA, and TcpT can be incorporated into cytoskeletal proteins to provide a real-time three-dimensional measurement of tension in IFs, MFs, and MTs when they "hang" on the cytoskeleton in astrocyte and U87 cells.

Intracellular steerable tension activity consists of OP, MF, and MT forces, while the GFAP tension can be regulated through their interaction [15]. Responding to an extracellular, gradually lowered hypo-osmotic gradient, the GFAP tension was enhanced progressively. When MFs and MTs were depolymerized, or molecular motors were inhibited, the GFAP tension was modified accordingly. Furthermore, the GFAP tension probe varied correspondingly in a glutamate-induced model of astrocytic swelling and could function as a rapid and valid indicator for the assessment of intracellular tension activity upon alterations of cell volume. Apart from the magnitude, the vector is another crucial property of intracellular tension activity and can be deduced through attenuating or eliminating certain cytoskeletal structural tensions under different conditions and comparing it with mechanical tensions. The interplay (vector relation) between the intracellular tensions during astrocytic swelling has been shown in Table 1. The studies suggest that inward contractile tensions of MF and MT act synergistically against outward OP in swollen astrocytes, contributing to protection during astrocyte swelling.
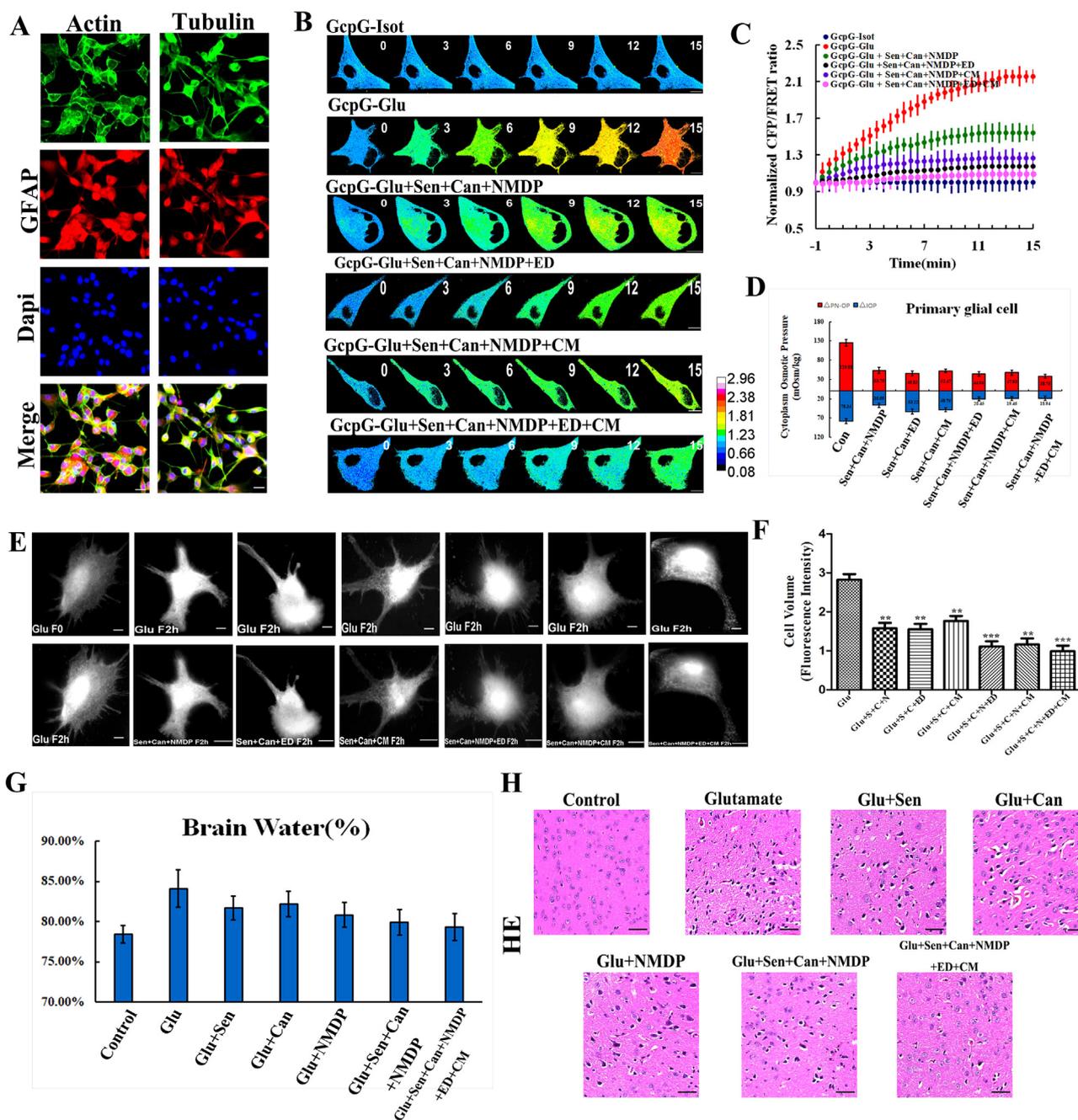
Fig. 8. Application of drug combinations after glutamate-induced astrocyte swelling in primary cultures. (A) Confocal laser microscopy was employed to analyze immunofluorescence staining for β-actin (FITC), α-tubulin (FITC), and GFAP (TRITC) in primary astrocytes. (B) GFAP tension was analyzed in primary astrocytes subjected to isotonic solution alone (row 1) and glutamate (row 2). The astrocyte swelling models were respectively treated with three drugs (row 3), four drugs (row 4 and 5), and five drugs combinations (row 6). The calibration bar was set from 0.08 to 2.96. (C) Normalized CFP/FRET signals of GFAP in the primary astrocyte swelling model with the treatment in Figure (B). (D) Effects of different drug combinations on glutamate-induced swelling of astrocytes in primary cell culture. The cytoplasm ion osmotic pressure (blue column) and protein nanoparticles-induced osmotic pressure (red column) were measured. (E) Calcein-fluorescence micrographs of primary glial cells at initially (F0) and at 2 h (F2h) in experiments with glutamate showing decreased *c*alcein fluorescence in membranes upon application of drug combinations. (F) Relative calcein fluorescence intensity compared with the effects of drugs. (G) The effect of drugs on neuroprotection was evaluated by brain water content after cytotoxic edema in rats. (H) Microscopic findings of cerebrum tissues revealed dense pericellular spaces, interstitial laxity, cytoplasmic condensation, and nuclear shrinkage. (H&E staining, ×20, arrowhead). Average of ≥ 3 experiments ± SEM.*p < 0.05, *p < 0.01, * **p < 0.001. (Scale bar = 20 μm.).

Glutamate is the primary excitatory amino acid neurotransmitter in the central nervous system and shows high levels after ischemic brain injury [29]. Glutamate stimulation results in cytotoxic astrocyte swelling in vitro and in vivo, accompanied by an increase in cytoplasmic OP. We found that glutamate signals resulted in depolymerization of MFs and MTs as well as the production of nanoparticles (actin and tubulin monomers or macromolecular polymers) that were involved in the production of cytoplasmic OP and PN-OP. This activity resulted from activation of their depolymerizing factors cofilin and stathmin-1, which are distributed widely in various tissues and dephosphorylation of which regulates their activation [56,57]. Cofilin was activated by SSH and calcium signals, whereas stathmin-1 was activated by PP2A, calcium signals, and PP2B [58–60]. Their activation contributes to an increase in cytoplasmic OP and PN-OP. Stabilization of MFs and MTs

Table 1

Vector relation between OP, MF, MT, and GFAP tensions. Vector analysis of the intracellular tension activity during astrocyte swelling in response to hypo-osmotic or glutamate treatment. In both circumstances, the inward MF and MT tension increase to antagonize the increment of outward GFAP tension in answer to OP, as indicated.

Treatment	Parameter	OP	MF tension	MT tension	GFAP tension	Phenomenon
Hypo-osmotic pressure	Magnitude	↑	↑	↑	↑	
	Vector	←	→	→	←	
Glutamate-induced swelling	Magnitude	↑	↑	↑	↑	Swell
	Vector	←	→	→	←	

↑indicates an increase; → shows an inward direction; ← shows an outward direction.

structure recovered the intracellular PN-OP and reduced the astrocyte swelling in response to glutamate stimulation, whereas attenuation of MF and MT tensions elicited by inhibitors of molecular motors exhibited no obvious effect. These data showed that cytoplasmic OP and PN-OP could be involved in glutamate-induced astrocyte swelling. Hence, cytoplasmic OP, especially PN-OP, is treated as drug targets to cure astrocyte swelling and brain edema.

Although, the PN-OP (used to known as colloid OP) had been thought to involved in intracellular tension activity according to the Van't Hoff theory, where protein granules enable generate osmotic pressure [61]. The Donnan effect might provide a reasonable explanation for the amplified role of protein nanoparticles-induced OP, which has been thoroughly discussed in the literature [37,44,45]. Disruption of the Donnan equilibrium generates the osmotic gradient across the plasma membrane. In physiologic pH circumstance, the protein nanoparticles like actin and α/β-tubulin carry negative charges and impart negative fixed charge density (FCD), which can strongly absorb mass positive ions near the colloidal surface [62,63]. Intracellular decreased free cation forms the osmolarities imbalance, drawing extracellular cations into the astrocytes. The cations accumulation would induce a charge gradient which leads to subsequent anions influx, ultimately brings about intracellular hyperosmosis and liquid inflow. Multiple numerical methods have been reported to support this theory, which evaluates how cell volume is affected by fixed charge density and the ion concentration in solutions [64–66]. The viewpoint also is supported by the present data. Firstly, production of protein nanoparticles can results markedly in upregulation of ion OP in response to depolymerization of MF and MT (Fig. 2). Secondly, MF and MT stabilizer or inhibitor of MF and MT depolymerization can effectively inhibit the increment of ion OP elicited by Glu stimuli (Fig. 4). Thirdly, the amount of intracellular protein nanoparticle produced and the OP increment reveal a significant linear relationship (Fig. 6). Fourthly, the inhibitor of anion channels or Na-K-Cl cotransporter has little effect on the decrease of IOP due to no elimination of protein nanoparticles. Based on this, the PN-OP could also be named as colloid-related OP, which is associated closely with their ion carrier.

Intracellular ion OP and PN-OP control the transmembrane osmotic gradient and aqueous influx during astrocyte swelling. To improve the treatment of clinical cerebral edema, the effect of some clinical drugs on intracellular OP was studied in the present study. A few Ca^{2+}-channel blockers Nimodipine, Cinepazide maleate, and Verapamil, the volume-regulated anion channels inhibitor Tamoxifen, and the Na-K-Cl cotransporter blocker bumetanide are employed to lower ion OP chiefly. The Shingshot inhibitor sennoside A, PP2A inhibitor cantharidin, ROCK inhibitor Y-27632 and fasudil are used to prevailingly lower PN-OP through inhibition of MF and MT depolymerization. Moreover, the neuroprotective agents such as Edaravone and Oxiracetam are employed to remove toxic substances like oxygen free radical. However, a single agent given individually could reduce intracellular total OP partly. Meanwhile, the cell volume and GFAP tension of glutamate-induced astrocyte swelling declined correspondingly in response to administration of certain drug combinations.

We also found that certain drugs could change the composition and properties of cytoplasmic ion OP and PN-OP, but the value of total OP

could not be reduced effectively. Therefore, astrocytic swelling could not be reversed. For example, treatment with the SSH inhibitor Sen resulted in a dose-dependent decrease in PN-OP accompanied by a simultaneous increase in ion OP. Intriguingly, the contrary phenomenon was observed upon administration of the ROCK inhibitor Y-27632. Furthermore, the free-radical scavenger edaravone and neuroprotective agent oxiracetam decreased ion OP and PN-OP distinctly, suggesting that elimination of intracellular toxic substances such as reactive oxygen species induced by glutamate could contribute to a reduction in cytoplasmic OP [10,68,69]. We speculated that cytotoxic astrocyte swelling might be a self-protection measure for diluting the toxic substances generated, similar to an inflammatory reaction. Our hypothesis was consistent with the results showing that elimination of accumulated Ca^{2+} toxicity via inhibition of Ca^{2+} channels contributed to relieve astrocyte swelling. The present study also suggests that the ratio of intracellular ion OP and PN-OP might be a crucial indicator for evaluating the drug therapy even if the value of total OP is unchanged.

The intracellular osmotic pressure, including ion OP and PN-OP, has been shown to be regulated synthetically by multi-factor. As a consequence, a plurality of drug targets should be simultaneously selected. A notable finding was that combined administration of regulators of PN-OP and ion OP could eliminate the cytoplasmic total OP effectively and cure astrocyte swelling. In the present study, we targeted at the MF depolymerizing factor cofilin, MT depolymerizing factor stathmin-1, and cellular toxicity induced by calcium overload and production of oxygen-derived free radicals. The most effective drugs combination was sennoside A + cantharidin + nimodipine + edaravone + cinepazide maleate, of which the optimum concentration (in μM) was 100, 2, 30, 50, and 10, respectively. This drug combination induced a remarkable decrease in the cytoplasmic OP, GFAP tension, and the volume of swollen astrocytes. This drug combination is also valid for primary glial cells and practical for rodent models of cerebral edema. The combination of the drugs can provide a new program for clinical treatment of cerebral edema.

5. Conclusions

The present study was designed to determine the role of intracellular tension activity in glutamate-induced astrocyte swelling. The magnitude and vectors of intracellular tension activity during astrocyte swelling was identified, in particular, protein nanoparticle-induced OP. Cytoplasmic OP and PN-OP could be generated by depolymerization of MFs and MTs, and production of protein nanoparticles resulting from activation of cofilin and stathmin-1. Also, ion OP and PN-OP could adjust reciprocally. Combined administration of regulators of the PN-OP and ion OP, as well as free-radical scavenger, could reduce cytoplasmic OP, recover cell volume, and improve ischemic brain lesions effectively. Recovery of cytoplasmic potential energy is a promising target to develop new drugs and cure brain edema. Further studies must be carried out to explore the mechanisms underlying intracellular ion OP and colloid-related OP and their interactions. The present study has provided more profound insights into the progression of astrocytic swelling and shed new light on treatment methods.

CRediT authorship contribution statement

JiaRui Zhang: Methodology, Data curation, Writing - original draft. **YuXuan Wang:** Writing - original draft, Methodology, Data curation. **ZiHui Zheng:** Writing - review & editing, Data curation. **XiaoHe Sun:** Methodology. **TingTing Chen:** Methodology. **Chen Li:** Methodology. **XiaoLong Zhang:** Methodology. **Jun Guo:** Project administration, Funding acquisition, Conceptualization.

Acknowledgments

Conflict of interest

The authors declare no competing interests

Appendix A. Supplementary material

Supplementary data associated with this article can be found in the online version at doi:10.1016/j.redox.2019.101112.

References

[1] S. Michinaga, Y. Koyama, Pathogenesis of brain edema and investigation into anti-edema drugs, Int. J. Mol. Sci. 16 (2015) 9949–9975.

[2] Z. Liu, M. Chopp, Astrocytes, therapeutic targets for neuroprotection and neurorestoration in ischemic stroke, Prog. Neurobiol. 144 (2016) 103–120.

[3] J. Sword, D. Croom, P.L. Wang, R.J. Thompson, S.A. Kirov, Neuronal pannexin-1 channels are not molecular routes of water influx during spreading depolarization-induced dendritic beading, J. Cerebr. Blood Flow Metab. 37 (2017) 1626–1633.

[4] N. Vardjan, A. Horvat, J.E. Anderson, D. Yu, D. Croom, X. Zeng, et al., Adrenergic activation attenuates astrocyte swelling induced by hypotonicity and neurotrauma, Glia 64 (2016) 1034–1049.

[5] J.A. Stokum, V. Gerzanich, J.M. Simard, Molecular pathophysiology of cerebral edema, J. Cereb. Blood Flow Metab. 36 (2016) 513–538.

[6] W.C. Risher, D. Croom, S.A. Kirov, Persistent astroglial swelling accompanies rapid reversible dendritic injury during stroke-induced spreading depolarizations, Glia 60 (2012) 1709–1720.

[7] Y.F. Wang, V. Parpura, Astroglial modulation of hydromineral balance and cerebral edema, Front. Mol. Neurosci. 11 (2018) 204.

[8] W. Yan, X. Zhao, H. Chen, D. Zhong, J. Jin, Q. Qin, et al., beta-dystroglycan cleavage by matrix metalloproteinase-2/-9 disturbs aquaporin-4 polarization and influences brain edema in acute cerebral ischemia, Neuroscience 326 (2016) 141–157.

[9] C. Rakers, M. Schmid, G.C. Petzold, TRPV4 channels contribute to calcium transients in astrocytes and neurons during peri-infarct depolarizations in a stroke model, Glia 65 (2017) 1550–1561.

[10] R. Reinehr, B. Gorg, S. Becker, N. Qvartskhava, H.J. Bidmon, O. Selbach, et al., Hypoosmotic swelling and ammonia increase oxidative stress by NADPH oxidase in cultured astrocytes and vital brain slices, Glia 55 (2007) 758–771.

[11] J.A. Stokum, M.S. Kwon, S.K. Woo, O. Tsymbalyuk, R. Vennekens, V. Gerzanich, et al., SUR1-TRPM4 and AQP4 form a heteromultimeric complex that amplifies ion/water osmotic coupling and drives astrocyte swelling, Glia 66 (2018) 108–125.

[12] R.L. Rungta, H.B. Choi, J.R. Tyson, A. Malik, L. Dissing-Olesen, P.J.C. Lin, et al., The cellular mechanisms of neuronal swelling underlying cytotoxic edema, Cell 161 (2015) 610–621.

[13] W. Dingyu, M. Fanjie, D. Zhengzheng, H. Baosheng, Y. Chao, P. Yi, et al., Regulation of intracellular structural tension by Talin in the axon growth and regeneration, Mol. Neurobiol. 53 (2016) 4582–4595.

[14] M.M. Maneshi, B. Maki, R. Gnanasambandam, S. Belin, G.K. Popescu, F. Sachs, et al., Mechanical stress activates NMDA receptors in the absence of agonists, Sci. Rep. 7 (2017) 39610 (Jan 3).

[15] Y.C. Guo, Y.X. Wang, Y.P. Ge, L.J. Yu, J. Guo, Analysis of subcellular structural tension in axonal growth of neurons, Rev. Neurosci. 29 (2018) 125–137.

[16] A.J. Kosmalska, L. Casares, A. Elosegui-Artola, J.J. Thottacherry, R. Moreno-Vicente, V. Gonzalez-Tarrago, et al., Physical principles of membrane remodelling during cell mechanoadaptation, Nat. Commun. 6 (2015) 7292.

[17] R.P. Martins, J.D. Finan, F. Guilak, D.A. Lee, Mechanical regulation of nuclear structure and function, Annu Rev. Biomed. Eng. 14 (2012) 431–455.

[18] M.I. Molodtsov, C. Mieck, J. Dobbelaere, A. Dammermann, S. Westermann, A. Vaziri, A force-induced directional switch of a molecular motor enables parallel microtubule bundle formation, Cell 167 (2016) 539–552 (e14).

[19] H.R. Thiam, P. Vargas, N. Carpi, C.L. Crespo, M. Raab, E. Terriac, et al., Perinuclear Arp2/3-driven actin polymerization enables nuclear deformation to facilitate cell migration through complex environments, Nat. Commun. 7 (2016) 10997.

[20] H. Li, Y.H. Zhu, C. Chi, H.W. Wu, J. Guo, Role of cytoskeleton in axonal regeneration after neurodegenerative diseases and CNS injury, Rev. Neurosci. 25 (2014) 527–542.

[21] C. Yang, X.H. Zhang, Y.C. Guo, F.J. Meng, F. Sachs, J. Guo, Mechanical dynamics in live cells and fluorescence-based force/tension sensors, Bba-Mol. Cell Res. 1853 (2015) 1889–1904.

[22] A.T. Lombardo, S.R. Nelson, M.Y. Ali, G.G. Kennedy, K.M. Trybus, S. Walcott, et al., Myosin Va molecular motors manoeuvre liposome cargo through suspended actin filament intersections in vitro, Nat. Commun. 8 (2017) 15692.

[23] T.T. Chen, Y.C. Guo, J.J. Shan, J.R. Zhang, X. Shen, J. Guo, et al., Vector analysis of cytoskeletal structural tension and the mechanisms that underpin Spectrin-related forces in pyroptosis, Antioxid. Redox Sign. (2018).

[24] D.A. Fletcher, D. Mullins, Cell mechanics and the cytoskeleton, Nature 463 (2010) 485–492.

[25] N. Caudron, I. Arnal, E. Buhler, D. Job, O. Valiron, Microtubule nucleation from stable tubulin oligomers, J. Biol. Chem. 277 (2002) 50973–50979.

[26] J.C. Drummond, Colloid osmotic pressure and the formation of posttraumatic cerebral edema, Anesthesiology 112 (2010) 1079–1081.

[27] M.C. Munder, D. Midtvedt, T. Franzmann, E. Nuske, O. Otto, M. Herbig, et al., A pH-driven transition of the cytoplasm from a fluid- to a solid-like state promotes entry into dormancy, Elife 5 (2016) e09347 (pii).

[28] K.V.R. Rao, A.R. Jayakumar, X.Y. Tong, V.M. Alvarez, M.D. Norenberg, Marked potentiation of cell swelling by cytokines in ammonia-sensitized cultured astrocytes, J. Neuroinflamm. 7 (2010) 66.

[29] Z.F. Shi, W. Zhang, Y. Lu, Y. Lu, L.X. Xu, Q. Fang, et al., Aquaporin 4-mediated glutamate-induced astrocyte swelling is partially mediated through metabotropic glutamate receptor 5 activation, Front. Cell Neurosci. 11 (2017) 116.

[30] J.M. Rutkowsky, B.K. Wallace, P.M. Wise, M.E. O'Donnell, Effects of estradiol on ischemic factor-induced astrocyte swelling and AQP4 protein abundance, Am. J. Physiol.-Cell Ph. 301 (2011) C204–C212.

[31] X.D. Sun, L. Li, F. Liu, Z.H. Huang, J.C. Bean, H.F. Jiao, et al., Lrp4 in astrocytes modulates glutamatergic transmission, Nat. Neurosci. 19 (2016) 1010–1018.

[32] S.R. Hinson, M.F. Romero, B.F.G. Popescu, C.F. Lucchinetti, J.P. Fryer, H. Wolburg, et al., Molecular outcomes of neuromyelitis optica (NMO)-IgG binding to aquaporin-4 in astrocytes, Proc. Natl. Acad. Sci. USA 109 (2012) 1245–1250.

[33] J. Guo, Y.X. Wang, F. Sachs, F.J. Meng, Actin stress in cell reprogramming, Proc. Natl. Acad. Sci. USA 111 (2014) E5252–E5261.

[34] V. Fineschi, R.V. Viola, R. La Russa, A. Santurro, P. Frati, A controversial medico-legal issue: the timing of onset of perinatal hypoxic-ischemic brain injury, Mediat Inflamm. 2017 (2017) 6024959.

[35] R. Min, M.S. van der Knaap, Genetic defects disrupting glial ion and water homeostasis in the brain, Brain Pathol. 28 (2018) 372–387.

[36] H.S. Muddana, R.R. Gullapalli, E. Manias, P.J. Butler, Atomistic simulation of lipid and DiI dynamics in membrane bilayers under tension, Phys. Chem. Chem. Phys. 13 (2011) 1368–1378.

[37] M.K. Nguyen, I. Kurtz, Quantitative interrelationship between Gibbs-Donnan equilibrium, osmolality of body fluid compartments, and plasma water sodium concentration, J. Appl. Physiol. 100 (2006) 1293–1300.

[38] R. Pigeat, P. Chausson, F.M. Dreyfus, N. Leresche, R.C. Lambert, Sleep slow wave-related homo and heterosynaptic LTD of intrathalamic GABAAergic synapses: involvement of T-type Ca2+ channels and metabotropic glutamate receptors, J. Neurosci. 35 (2015) 64–73.

[39] A.S. Thrane, V. Rangroo Thrane, M. Nedergaard, Drowning stars: reassessing the role of astrocytes in brain edema, Trends Neurosci. 37 (2014) 620–628.

[40] C. Wippel, J. Maurer, C. Fortsch, S. Hupp, A. Bohl, J. Ma, et al., Bacterial cytolysin during meningitis disrupts the regulation of glutamate in the brain, leading to synaptic damage, PLoS Pathog. 9 (2013) e1003380.

[41] C.Y. Chang, J.D. Leu, Y.J. Lee, The actin depolymerizing factor (ADF)/cofilin signaling pathway and DNA damage responses in cancer, Int J. Mol. Sci. 16 (2015) 4095–4120.

[42] K.K. Gupta, C.L. Li, A. Duan, E.O. Alberico, O.V. Kim, M.S. Alber, et al., Mechanism for the catastrophe-promoting activity of the microtubule destabilizer Op18/stathmin, P Natl. Acad. Sci. USA 110 (2013) 20449–20454.

[43] C. Juliano, G. Galleri, T. Klemetsrud, J. Karlsen, P. Giunchedi, Effect of chitosan malate on viability and cytoskeletal structures morphology of Caco-2 cells, Int J. Pharm. 420 (2011) 223–230.

[44] G.E. Lang, P.S. Stewart, D. Vella, S.L. Waters, A. Goriely, Is the Donnan effect sufficient to explain swelling in brain tissue slices? J. R. Soc. Interface 11 (2014) 20140123.

[45] S. Kurbel, Are extracellular osmolality and sodium concentration determined by Donnan effects of intracellular protein charges and of pumped sodium? J. Theor. Biol. 252 (2008) 769–772.

[46] A.H. Qian, D.D. Song, Y. Li, X.Q. Liu, D. Tang, W.Y. Yao, et al., Role of voltage gated Ca2+ channels in rat visceral hypersensitivity change induced by 2,4,6-trinitrobenzene sulfonic acid, Mol. Pain. 9 (2013) 15.

[47] J.W. Hell, How Ca2+-permeable AMPA receptors, the kinase PKA, and the phosphatase PP2B are intertwined in synaptic LTP and LTD, Sci. Signal. 9 (2016) e2.

[48] K. Okamura, T. Tsubokawa, H. Johshita, H. Miyazaki, Y. Shiokawa, Edaravone, a free radical scavenger, attenuates cerebral infarction and hemorrhagic infarction in

rats with hyperglycemia, Neurol. Res. 36 (2014) 65–69.

[49] Y.H. Zhang, H.Q. Zhang, P.J. Feustel, H.K. Kimelberg, DCPIB, a specific inhibitor of volume regulated anion channels (VRACs), reduces infarct size in MCAo and the release of glutamate in the ischemic cortical penumbra, Exp. Neurol. 210 (2008) 514–520.

[50] A.R. Jayakumar, X.Y. Tong, R. Ruiz-Cordero, A. Bregy, J.R. Bethea, H.M. Bramlett, et al., Activation of NF-kappaB mediates astrocyte swelling and brain edema in traumatic brain injury, J. Neurotrauma 31 (2014) 1249–1257.

[51] T.T. Song, Y.H. Bi, Y.Q. Gao, R. Huang, K. Hao, G. Xu, et al., Systemic pro-inflammatory response facilitates the development of cerebral edema during short hypoxia, J. Neuroinflamm. (2016) 13.

[52] A.R. Jayakumar, K.V.R. Rao, X.Y.Y. Tong, M.D. Norenberg, Calcium in the mechanism of ammonia-induced astrocyte swelling, J. Neurochem. 109 (2009) 252–257.

[53] J.A. Stokum, D.B. Kurland, V. Gerzanich, J.M. Simard, Mechanisms of astrocyte-mediated cerebral edema, Neurochem. Res. 40 (2015) 317–328.

[54] X. Cheng, P.M. Pinsky, The balance of fluid and osmotic pressures across active biological membranes with application to the corneal endothelium, PLoS One 10 (2015) e0145422.

[55] T.J. Jentsch, VRACs and other ion channels and transporters in the regulation of cell volume and beyond, Nat. Rev. Mol. Cell Bio. 17 (2016) 293–307.

[56] R. Adachi, K. Takeuchi, K. Suzuki, Antisense oligonucleotide to cofilin enhances respiratory burst and phagocytosis in opsonized zymosan-stimulated mouse macrophage J774.1 cells, J. Biol. Chem. 277 (2002) 45566–45571.

[57] S. Chauvin, A. Sobel, Neuronal stathmins: a family of phosphoproteins cooperating for neuronal development, plasticity and regeneration, Progress. Neurobiol. 126 (2015) 1–18.

[58] Y. Yamashiro, C.L. Papke, J. Kim, L.J. Ringuette, Q.J. Zhang, Z.P. Liu, et al., Abnormal mechanosensing and cofilin activation promotes the progression of ascending aortic aneurysms in mice, Sci. Signal. 8 (2015).

[59] E. Alli, J.M. Yang, J.M. Ford, W.N. Hait, Reversal of stathmin-mediated resistance to paclitaxel and vinblastine in human breast carcinoma cells, Mol. Pharmacol. 71 (2007) 1233–1240.

[60] N. Ohkawa, K. Fujitani, E. Tokunaga, S. Furuya, K. Inokuchi, The microtubule de-stabilizer stathmin mediates the development of dendritic arbors in neuronal cells, J. Cell Sci. 120 (2007) 1447–1456.

[61] Y. Lu, L.X. Wang, D.J. Chen, G.K. Wang, Determination of the concentration and the average number of gold atoms in a gold nanoparticle by osmotic pressure, Langmuir 28 (2012) 9282–9287.

[62] L.M. Wang, M.Y. Li, Y. Xie, L.L. Xu, R.D. Ye, X.F. Liu, Preclinical efficacy of human albumin in Subarachnoid Hemorrhage, Neuroscience 344 (2017) 255–264.

[63] B.S. Elkin, M.A. Shaik, B. Morrison, Fixed negative charge and the Donnan effect: a description of the driving forces associated with brain tissue swelling and oedema, Philos. T R. Soc. A. 368 (2010) 585–603.

[64] T.E. Colla, A.P. dos Santos, Y. Levin, Equation of state of charged colloidal suspensions and its dependence on the thermodynamic route, J. Chem. Phys. 136 (2012) 194103.

[65] P.C. Chao, M. Sivaselvan, F. Sachs, Cytoskeletal contribution to cell stiffness due to osmotic swelling; extending the donnan equilibrium, Curr. Top. Membr. 81 (2018) 83–96.

[66] G.A. Ateshian, S. Maas, J.A. Weiss, Multiphasic finite element framework for modeling hydrated mixtures With multiple neutral and charged solutes, J. Biomech. Eng.-T Asme 135 (2013) 111001.

[67] F. Sachs, M.V. Sivaselvan, Cell volume control in three dimensions: water movement without solute movement, J. Gen. Physiol. 145 (2015) 373–380.

[68] W. Li, H.H. Liu, H.J. Jiang, C. Wang, Y.F. Guo, Y. Sun, et al., (S)-Oxiracetam is the active ingredient in oxiracetam that alleviates the cognitive impairment induced by chronic cerebral hypoperfusion in rats, Sci. Rep. 7 (2017) 10052.

[69] J.M. Yoo, B.D. Lee, D.E. Sok, J.Y. Ma, M.R. Kim, Neuroprotective action of N-acetyl serotonin in oxidative stress-induced apoptosis through the activation of both TrkB/CREB/BDNF pathway and Akt/Nrf2/Antioxidant enzyme in neuronal cells, Redox Biol. 11 (2017) 592–599.